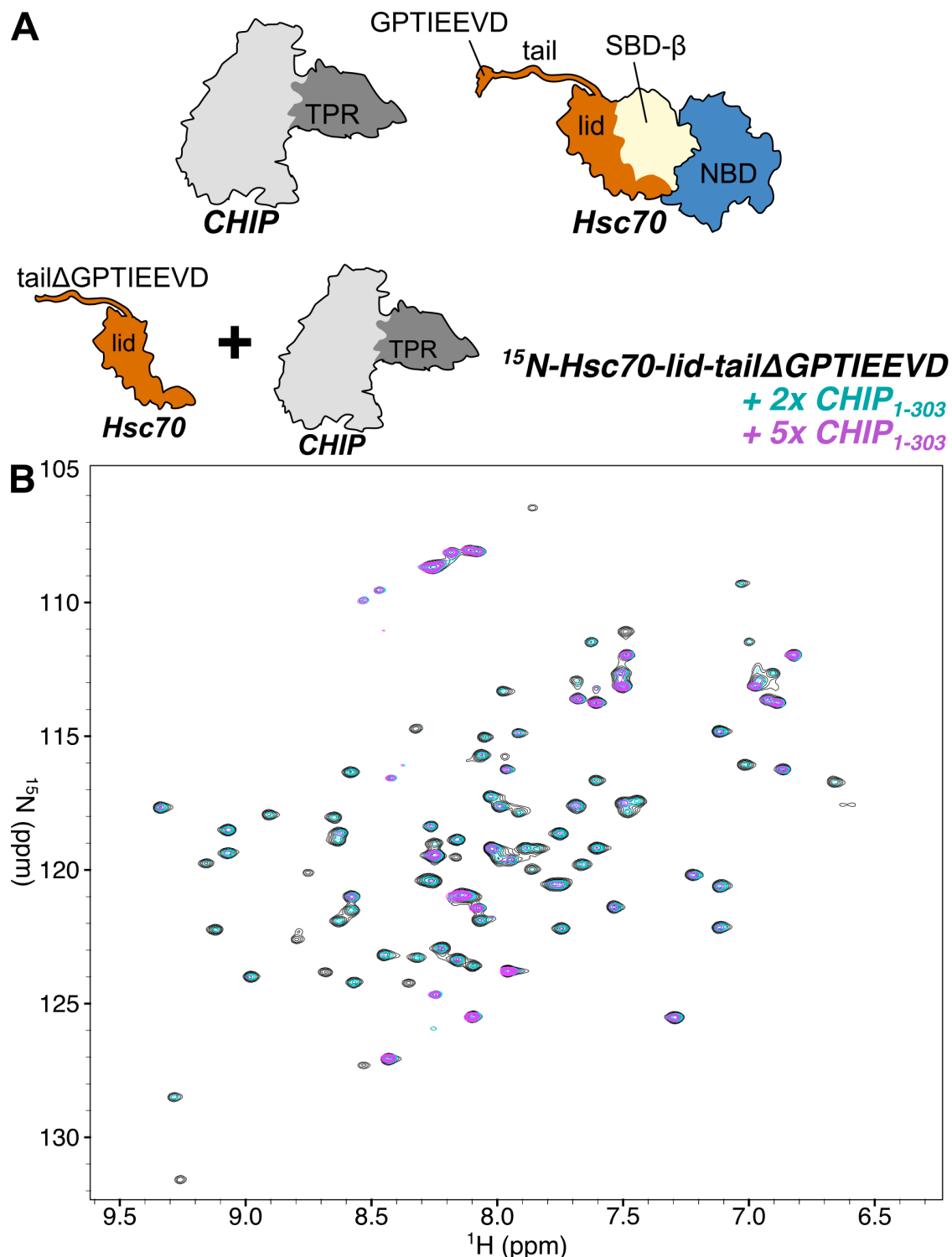
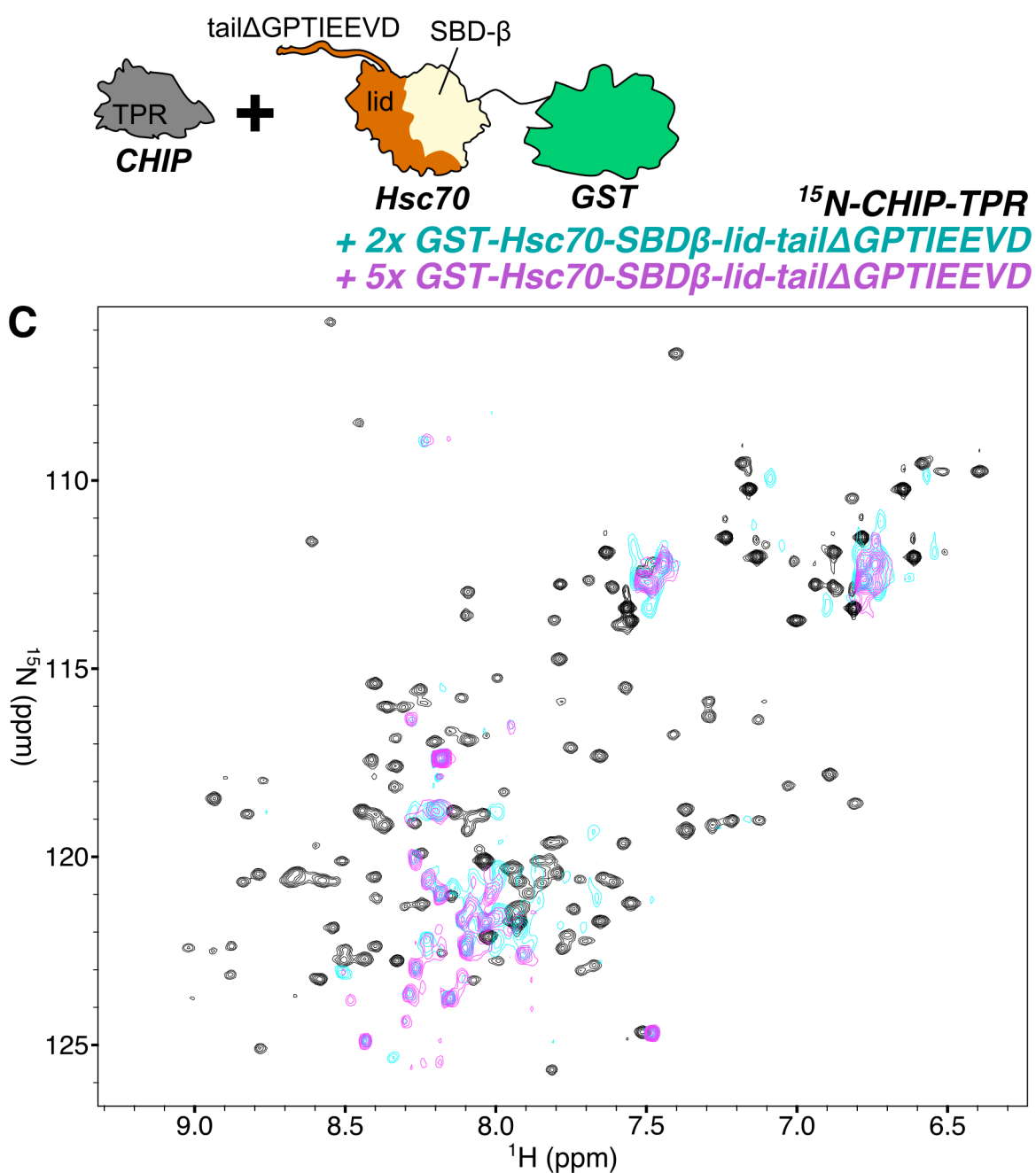


## Supplemental Figures and Legends



**Figure S1, related to Figure 1. HSQC-NMR titrations identify interactions between CHIP-TPR and the Hsc70-lid-tail.** (A) Schematic of CHIP and Hsc70 domains to aid identification of domains utilized in HSQC titrations. (B)  $^1\text{H}/^{15}\text{N}$ - Hsc70-lid-tail $\Delta$ GPTIEEVD was titrated with 2x and 5x molar excesses of full-length CHIP resulting in significant line broadening.  $^{15}\text{N}$ -Hsc70-lid-tail $\Delta$ GPTIEEVD concentrations began at 100  $\mu\text{M}$  and finished at  $\sim 75 \mu\text{M}$



**Figure S1, related to Figure 1 (continued). HSQC-NMR titrations identify interactions between CHIP-TPR and Hsc70-lid-tail.** (C) Titration of  $^1\text{H}/^{15}\text{N}$ -HsCHIP-TPR with 2x and 5x molar excesses of GST~Hsc70-lid-tail $\Delta$ GPTIEEVD caused extensive line broadening.  $^{15}\text{N}$ -CHIP-TPR concentrations began at 100  $\mu\text{M}$  and finished at  $\sim$ 80  $\mu\text{M}$ .

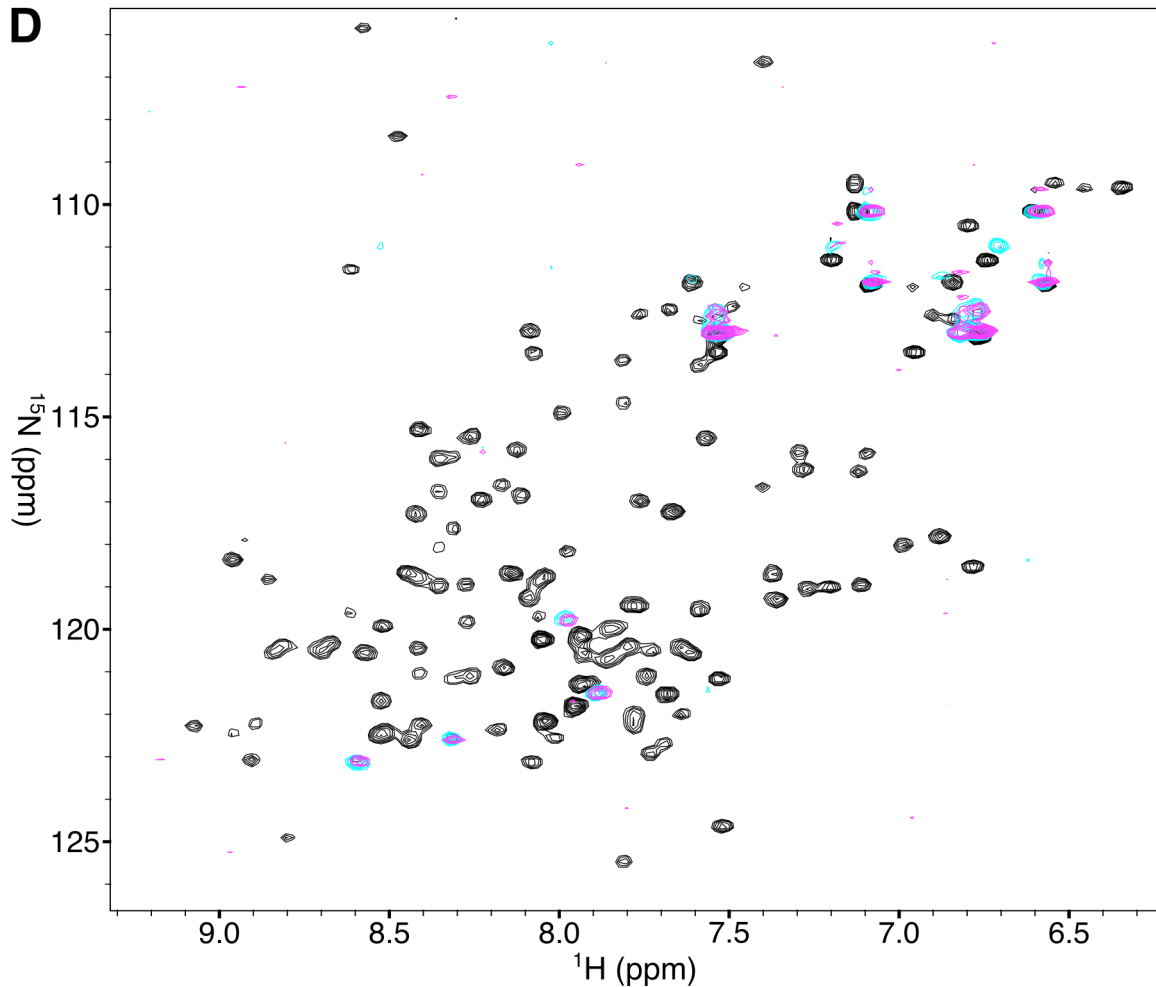
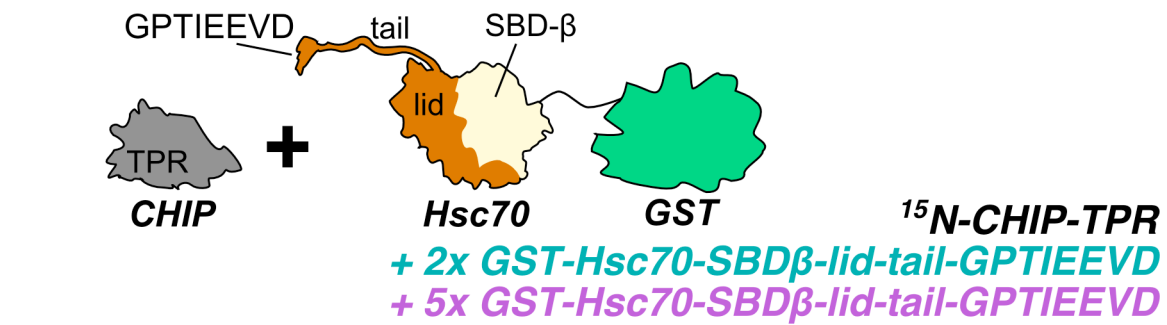


**Figure S1, related to Figure 1 (continued). HSQC-NMR titrations identify interactions between CHIP-TPR and Hsc70-lid-tail.** (D) Titration of  $^1\text{H}/^{15}\text{N}$ -HsCHIP-TPR with 2x and 5x molar excesses of GST~Hsc70-lid-tail-GPTIEEVD caused extensive line broadening.  $^{15}\text{N}$ -CHIP-TPR concentrations began at 100  $\mu\text{M}$  and finished at  $\sim 85$   $\mu\text{M}$ .

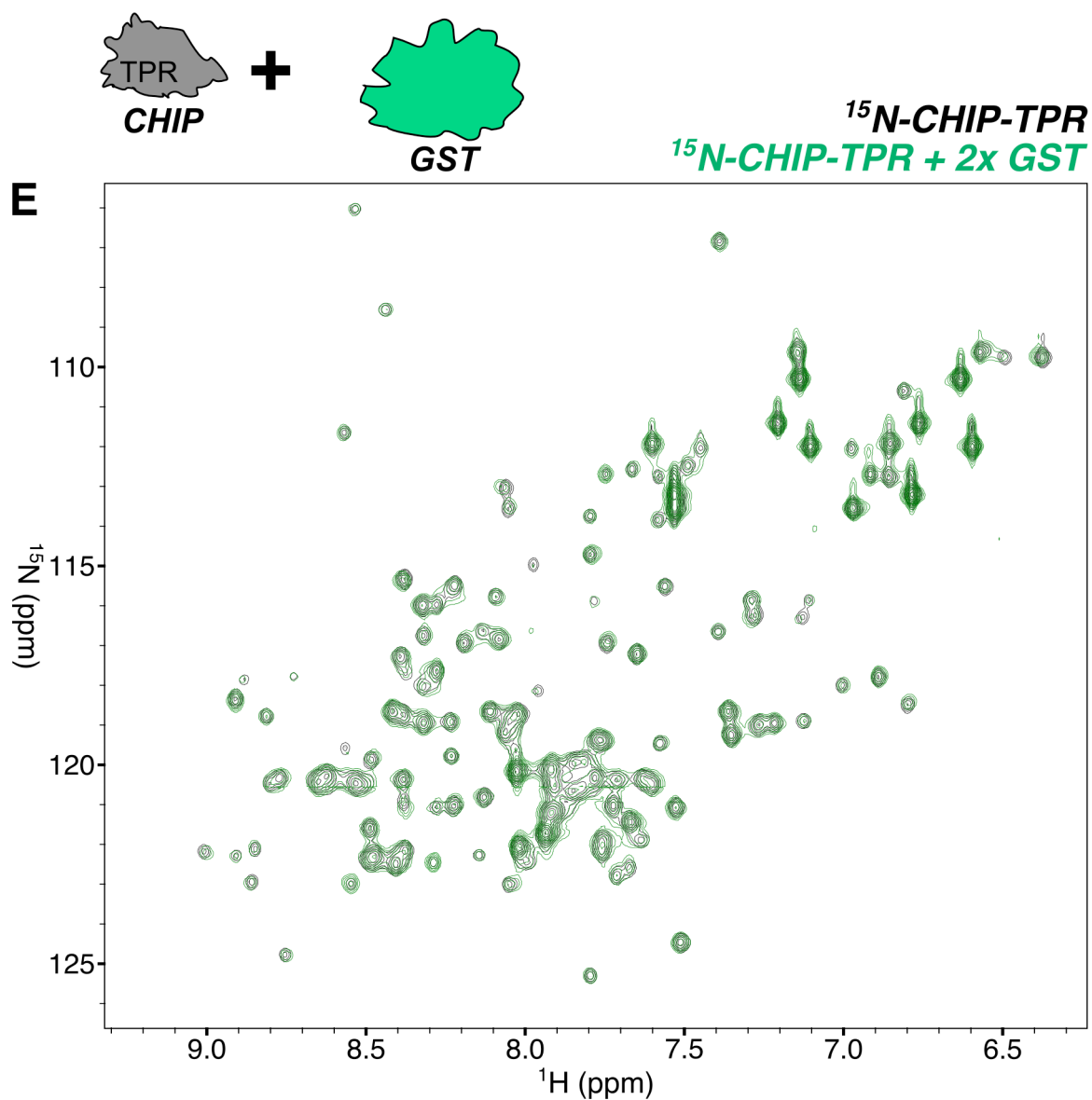


**Figure S1, related to Figure 1 (continued). HSQC-NMR titrations identify interactions between CHIP-TPR and Hsc70-lid-tail.** (E)  $^1\text{H}/^{15}\text{N}$ -CHIP-TPR titrated with a 10x molar excess of GST. Minimal chemical shift perturbations are observed.  $^{15}\text{N}$ -CHIP-TPR concentrations began at 100  $\mu\text{M}$  and finished at  $\sim 90$   $\mu\text{M}$ .



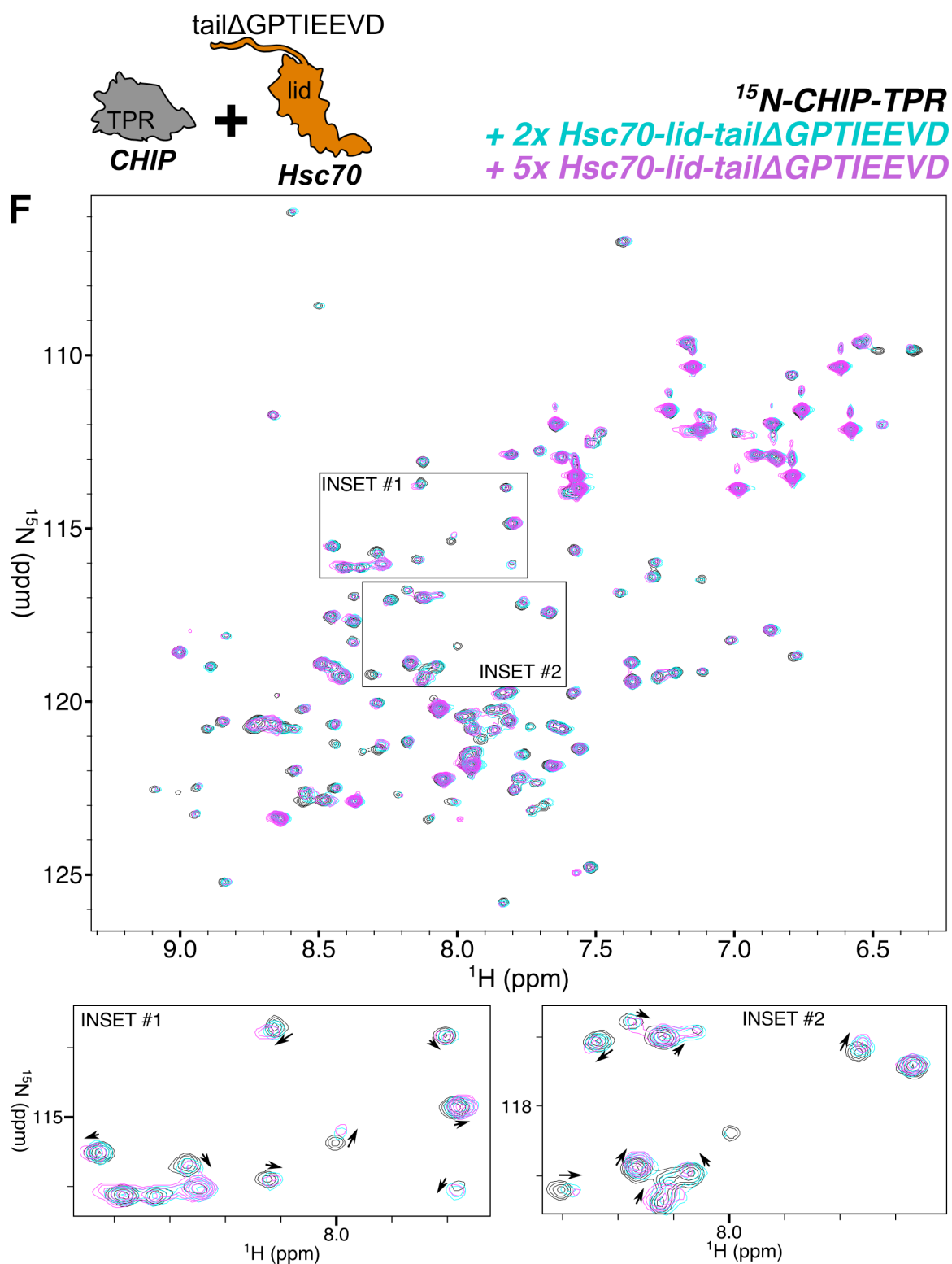


**Figure S1, related to Figure 1 (continued). HSQC-NMR titrations identify interactions between CHIP-TPR and Hsc70-lid.** (F) 2x and 5x molar excesses of unlabeled Hsc70-lid-tail $\Delta$ GPTIEEVD titrated into <sup>1</sup>H/<sup>15</sup>N-CHIP-TPR induce chemical shift perturbations and broadening of selected resonances. <sup>15</sup>N-CHIP-TPR concentrations began at 200  $\mu$ M and finished at  $\sim$ 110  $\mu$ M.

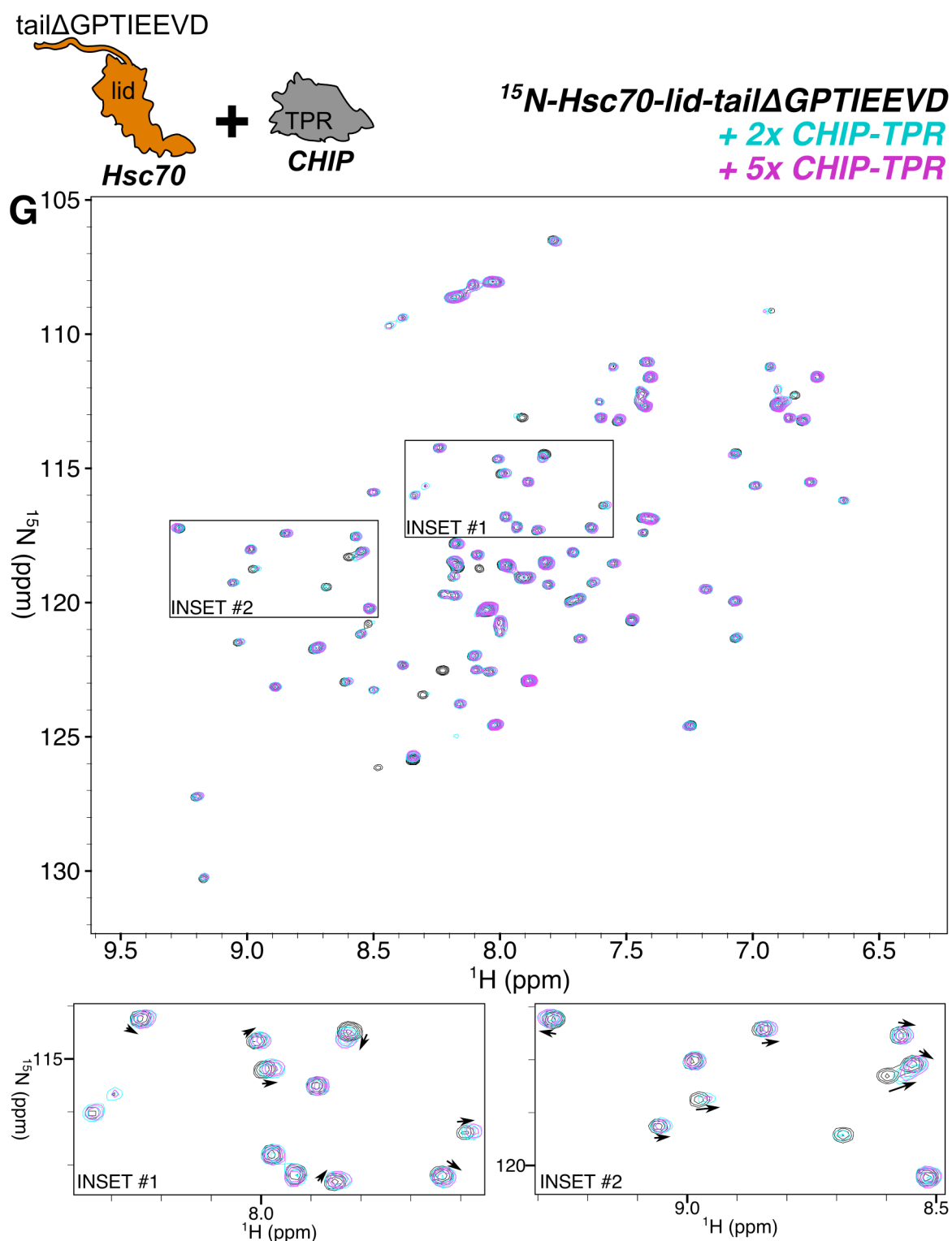


**Figure S1, related to Figure 1 (continued). HSQC-NMR titrations identify interactions between CHIP-TPR and Hsc70-lid-tail.** (G)  $^1\text{H}/^{15}\text{N}$ -Hsc70-lid-tail $\Delta$ GPTIEEVD titrated with 2x and 5x molar excesses of unlabeled CHIP-TPR lead to chemical shift perturbations and line broadening for a subset of resonances.  $^{15}\text{N}$ -Hsc70-lid-tail $\Delta$ GPTIEEVD concentrations began at 200  $\mu\text{M}$  and finished at  $\sim 150$   $\mu\text{M}$ .

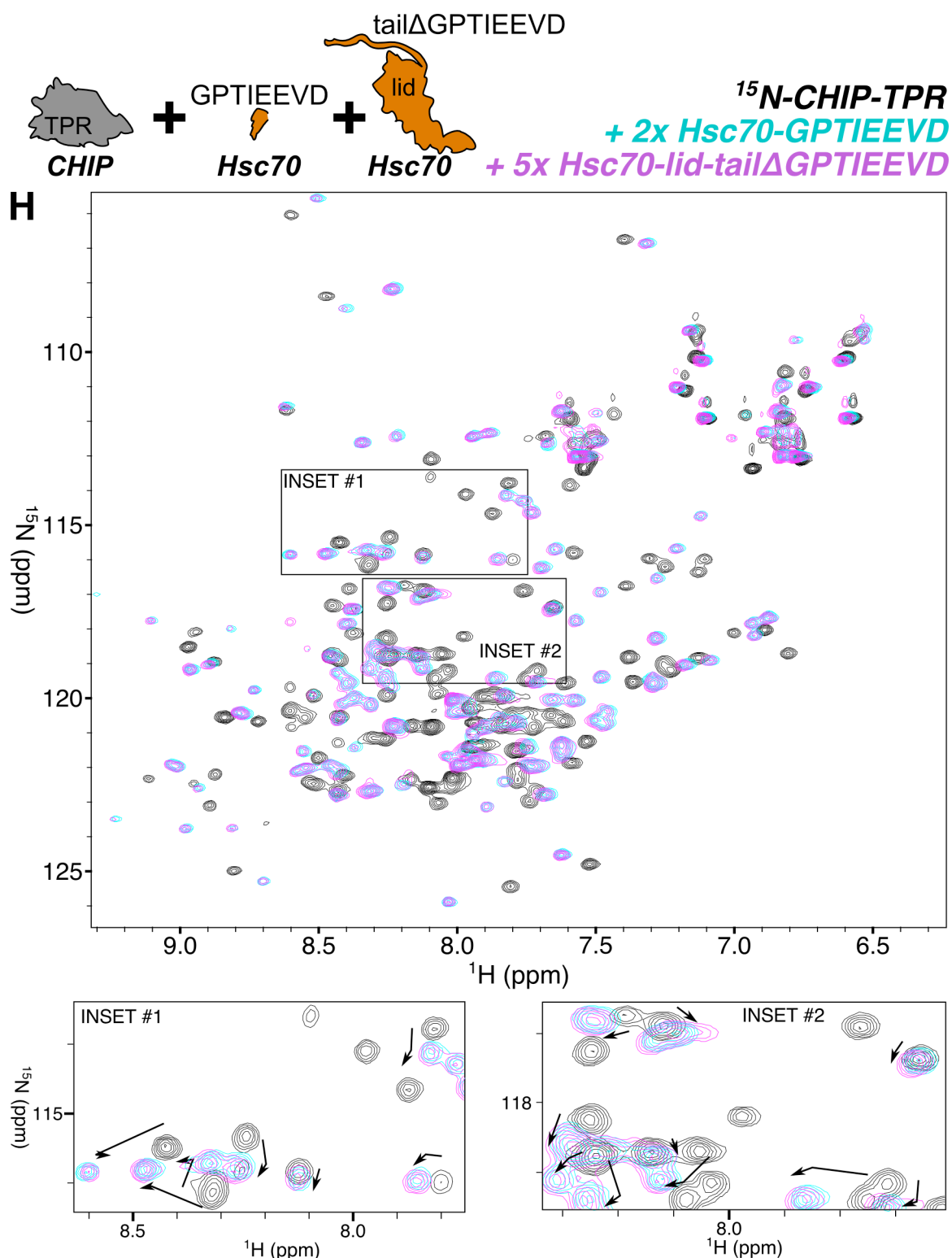


**Figure S1, related to Figure 1 (continued). HSQC-NMR titrations identify simultaneous interactions between CHIP-TPR, Hsc70-lid-tail and Hsc70-IEEVD.** (H)  $^1\text{H}/^{15}\text{N}$ -CHIP-TPR titrated with a 2x molar excess of unlabeled Hsc70-IEEVD leads to slow exchange chemical shift perturbations. Addition of a 5x molar excess of unlabeled Hsc70-lid-tail $\Delta$ GPTIEEVD leads to additional fast exchange chemical shift perturbations and line broadening for a subset of resonances.  $^{15}\text{N}$ -CHIP-TPR concentrations began at 100  $\mu\text{M}$  and finished at  $\sim 80 \mu\text{M}$ .

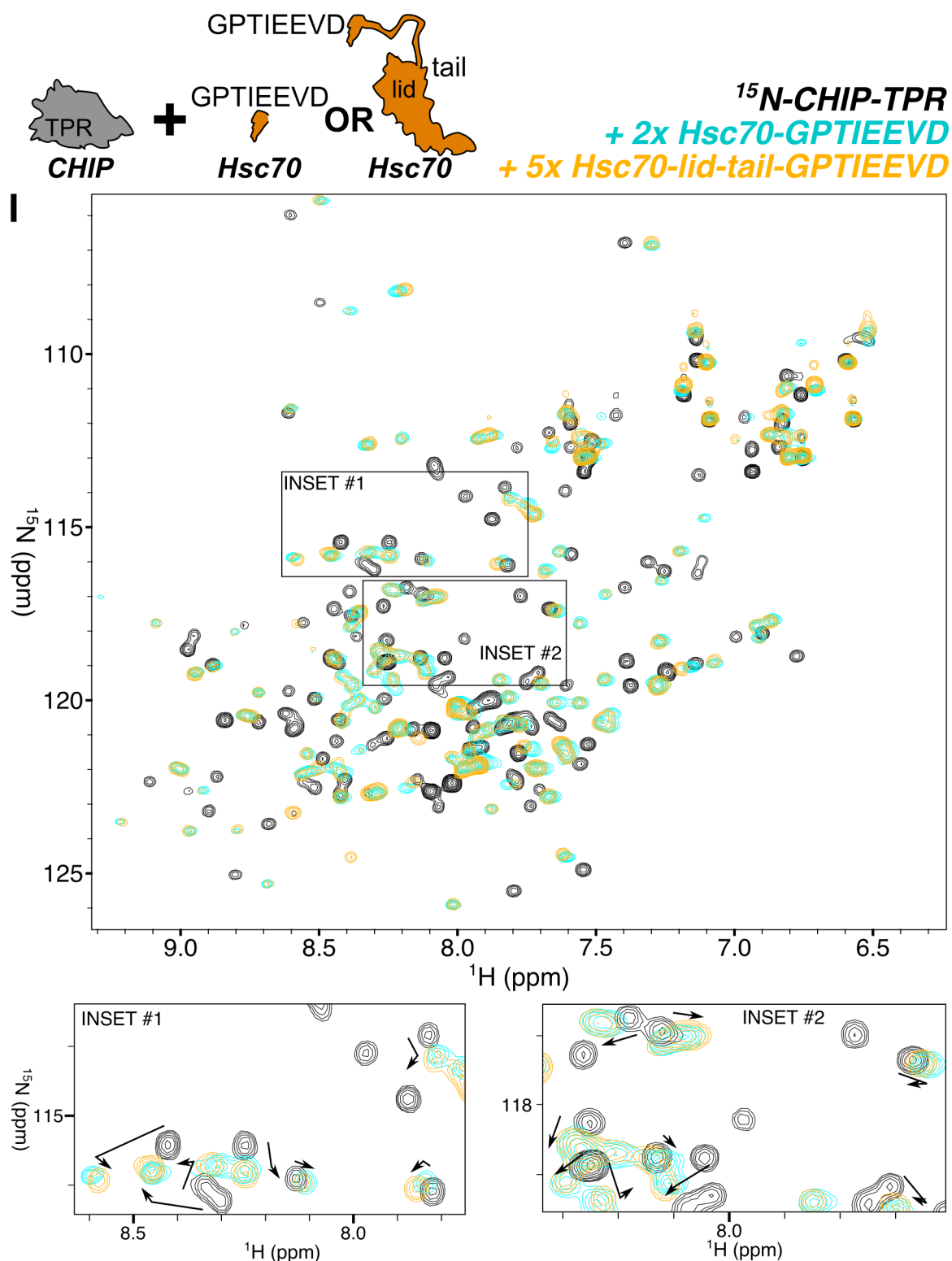


**Figure S1, related to Figure 1 (continued). HSQC-NMR titrations identify interactions between CHIP-TPR and Hsc70-lid-tail-IEEVD.** (I) In comparison to titration with Hsc70-IEEVD, titration a separate  $^1\text{H}/^{15}\text{N}$ -CHIP-TPR sample with a 5x molar excess of unlabeled Hsc70-lid-tail-GPTIEEVD leads to additional fast exchange chemical shift perturbations and line broadening for a subset of resonances similar to those observed in Figure S1H.  $^{15}\text{N}$ -CHIP-TPR concentrations began at 100  $\mu\text{M}$  and finished at  $\sim 85$   $\mu\text{M}$ .

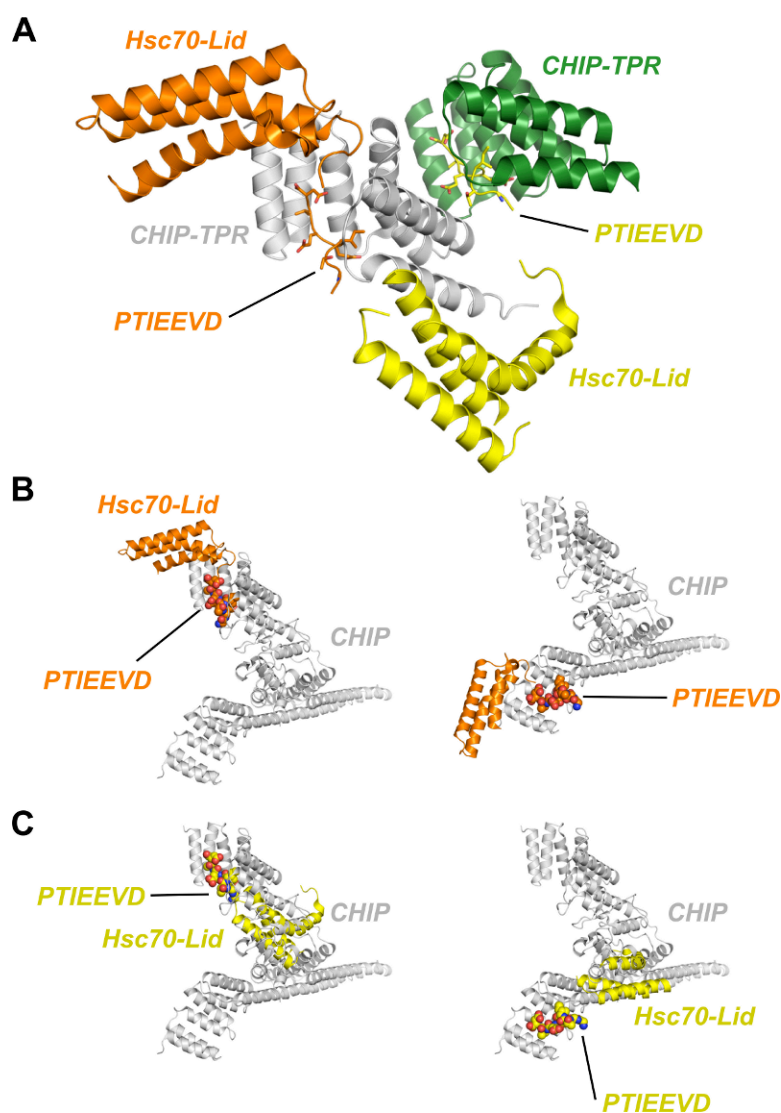


**Figure S2, related to Figure 1. Two different orientations of Hsc70-Lid are observed in the crystal structure.** (A) The asymmetric unit contains two copies each of HsCHIP<sub>21-154</sub> and HsHsc70<sub>541-646</sub>Δ<sub>626-638</sub>. The Hsc70-Lid in orange between “chain A” and “chain C” (orange, HsHsc70<sub>541-646</sub>Δ<sub>626-638</sub>) makes extensive contacts with one of the CHIP-TPRs (grey, HsCHIP<sub>21-154</sub>) with total buried surface area of ~485 Å<sup>2</sup> (per partner). The other Hsc70-Lid (yellow) makes more limited contacts with the same CHIP-TPR, burying 255 Å<sup>2</sup> per partner. (B) The primary lid orientation is fully compatible with binding to the full-length CHIP dimer (PDB code 2c2l; (Zhang et al., 2005) and induces no steric clashes when bound to either protomer of the CHIP dimer. (C) The secondary lid orientation is incompatible with binding to either protomer of a full-length CHIP dimer due to extensive steric clashes. Buried surface area calculations performed in PISA (Krissinel and Henrick, 2007). Molecular images rendered using PyMOL (Schrödinger LLC.).

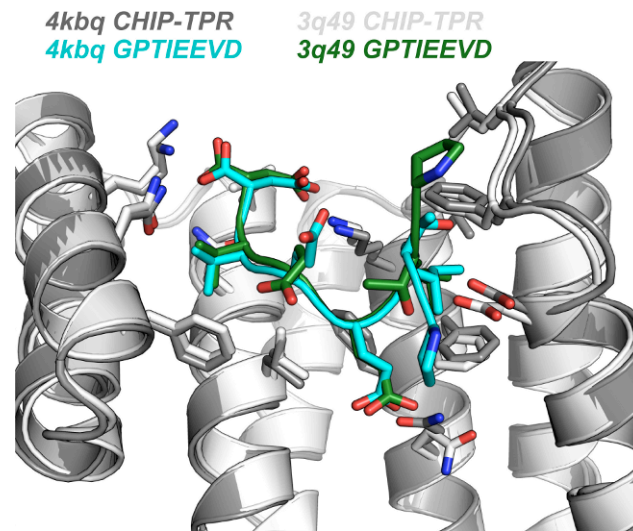


**Figure S3, related to Figure 1. Two different orientations of Pro<sub>640</sub> within the Hsc70-PTIEEVD are observed in the crystal structures.** While the position of the terminal aspartate and two-carboxylate clamp are identical, small variations in peptide orientation are observed between a structure of CHIP-TPR in complex with a GPTIEEVD peptide (PDB ID 3q49; Wang et al., 2011) and the structure of Hsc70-lid+tail presented here (PDB ID 4kbq). The two peptide orientations diverge most at Pro<sub>640</sub>, which makes limited contacts with the CHIP-TPR in each structure.

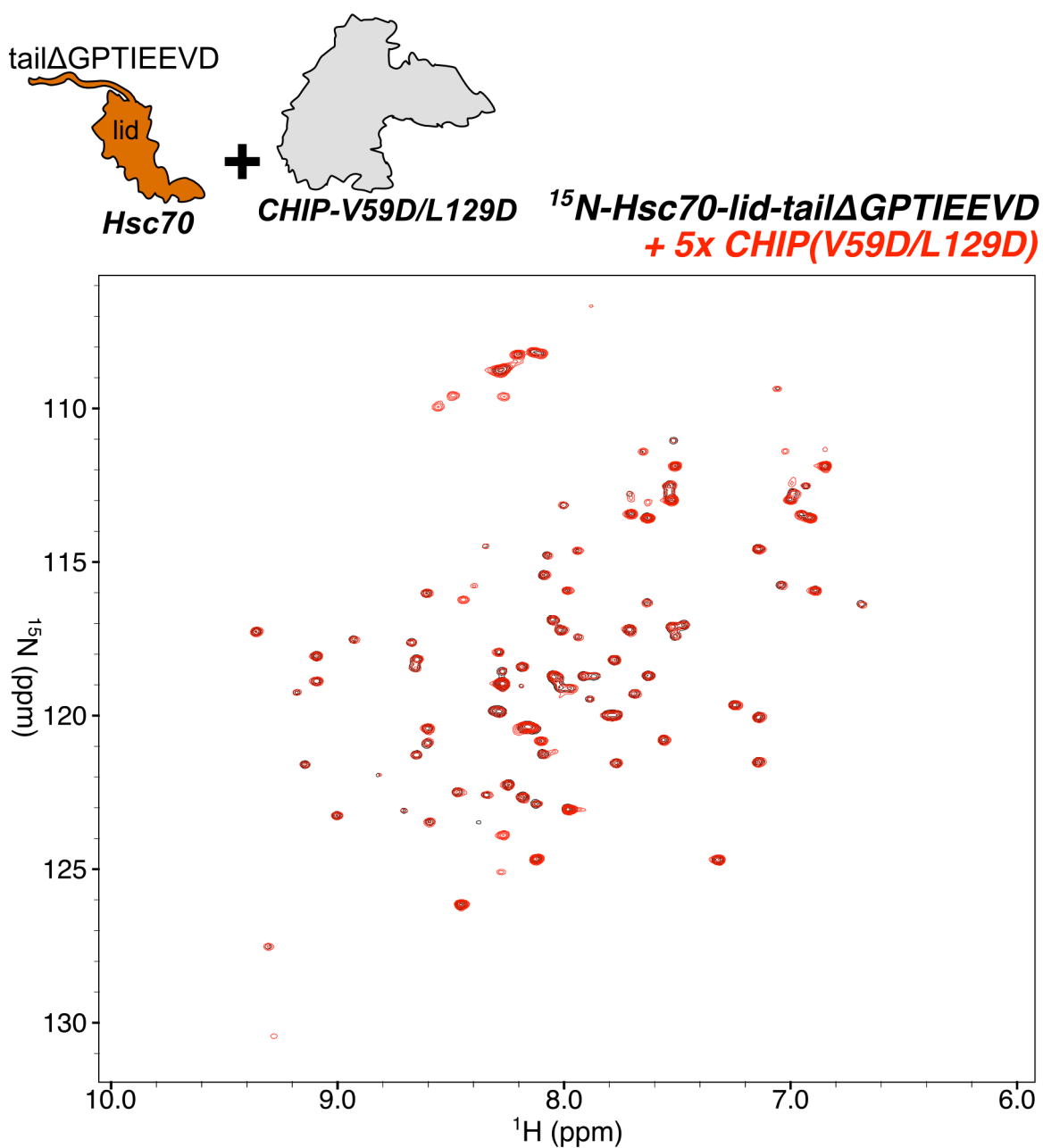


**Figure S4, related to Figure 2. Disruption of the lid/TPR interaction in ubiquitination-defective CHIP mutants.** Titration of  $^1$ H/ $^{15}$ N-Hsc70-lid-tail $\Delta$ GPTIEEVD with a 5x molar excess of full-length  $^{15}$ N-CHIP<sub>V59D/L129D</sub> causes little or no line broadening and no chemical shift perturbations.  $^{15}$ N-Hsc70-lid-tail $\Delta$ GPTIEEVD concentrations began at 100  $\mu$ M and finished at  $\sim$ 70  $\mu$ M.



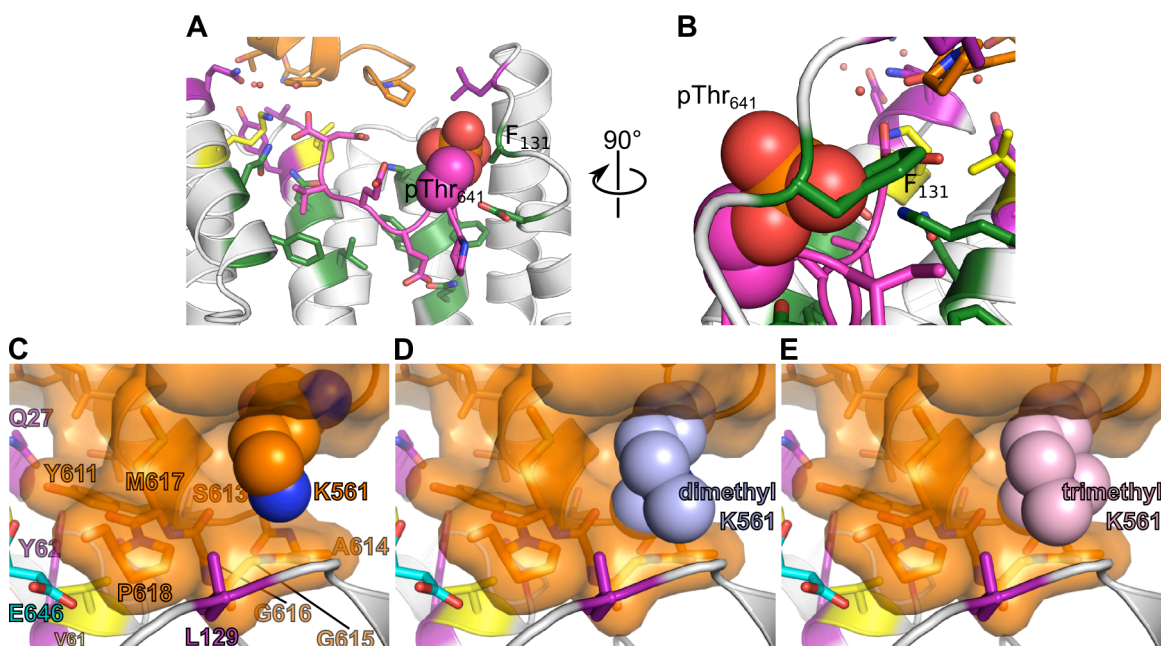


**Figure S5, related to Figure 5. Model of the CHIP-TPR domain complex with the post-translationally modified Hsc70.** (A) The phosphate group of pT641 may clash or interact unfavorably with residues near the 7<sup>th</sup> helix of the TPR domain, in particular with CHIP F131. (B) Zoomed and rotated view of the pT641/F131 clash. (C) Hsc70-K561 packs against the surface of the extended loop formed by residues 613-618. (D) Model of dimethyl-K561 identifies clashes between a K561-N-methyl group and extended loop. (E) Model of trimethyl-K561 identifies clashes between a K561-N-methyl group and extended loop.



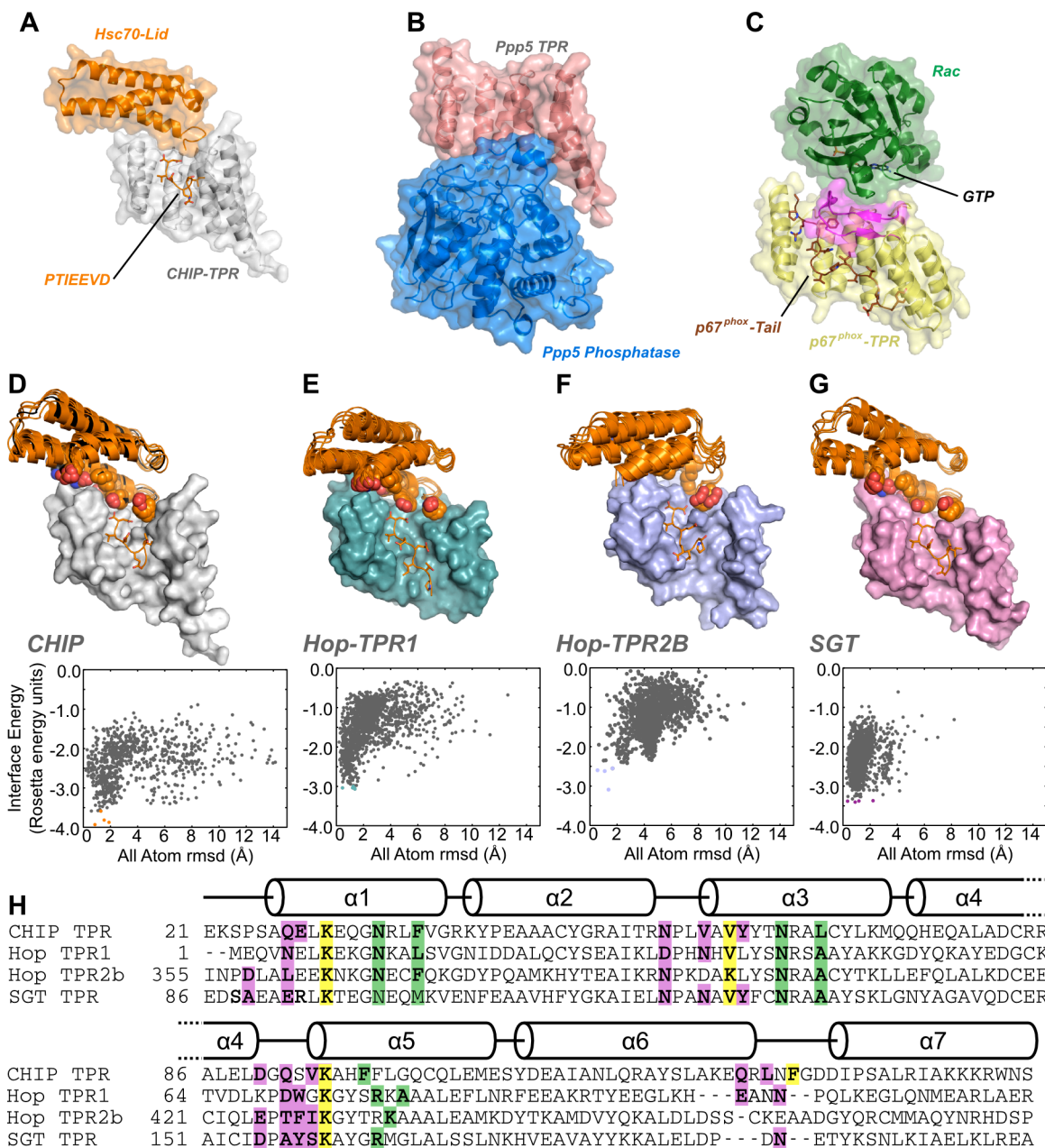


**Figure S6, related to Figure 6. Comparison between the TPR:Hsc70-lid-tail interactions and other TPR interactions with globular domains.** (A) The Hsc70-lid-tail (orange) binds to CHIP-TPR (grey) through a two-carboxylate clamp peptide binding mode and interactions between the lid and inter-TPR loops of CHIP. (B) The phosphatase domain of Ppp5a (pink) interacts with the Ppp5a TPR (light blue) via interactions with inter-TPR loops and the peptide binding groove is open (Yang et al., 2005). (C) Rac GTPase interacts with the p67<sup>phox</sup>-TPR (yellow) via interactions with inter-TPR loops (magenta); however, the p67<sup>phox</sup>-TPR superhelical groove is occupied by the carboxy-terminal sequence of p67<sup>phox</sup> (brown, Lapouge et al., 2000). (D) Rosetta Dock low energy decoy cluster for the CHIP-TPR (grey) in complex with Hsc70-lid-tail (orange). TPR domains are shown in surface representation. The five lowest energy Hsc70-lid-tail decoys are drawn as cartoons. Side-chain atoms for CHIP-TPR-interacting residues of Hsc70-lid are drawn as spheres. A plot of interface energy versus

all atom rmsd to the lowest energy decoy is shown beneath each cluster. For the CHIP-TPR:Hsc70-lid-tail complex, all atom rmsd was calculated against CHIP-TPR:Hsc70-lid-tail crystal structure. (E) Low energy cluster for the Hop-TPR1 (turquoise, Scheufler et al., 2000) in complex with Hsc70-lid-tail (orange). (F) Low energy cluster for the Hop-TPR2B (blue, Schmid et al., 2012) in complex with Hsc70-lid-tail (orange). (G) Low energy cluster for the SGT-TPR (pink, Dutta and Tan, 2008) in complex with Hsc70-lid-tail (orange). (H) Sequence alignment of CHIP-TPR, Hop-TPR1, and Hop-TPR2B domains with secondary structure overlay. Residues interacting with the Hsc70-lid, Hsc70-GPTIEEVD motifs, or both, are colored purple, green and yellow respectively.

**Supplemental Experimental Procedures***Materials*

Rabbit anti-CHIP, mouse anti-CHIP, Rabbit anti-GST and mouse anti-GST polyclonal antibodies were purchased from Sigma. Goat polyclonal anti-CHIP antibody was purchased from Millipore. Rabbit monoclonal anti-GFP and polyclonal anti- $\beta$ -actin were purchased from Cell Signaling and Thermo respectively. Mouse anti-iNOS and anti-GAPDH polyclonals were purchased from BD Transduction Laboratories and Fitzgerald Industries, respectively. Goat anti-mouse 800CW, Donkey anti-Rabbit 680LT and Donkey anti-goat 680 LT IRDye-labeled secondary antibodies were obtained from LI-COR. Ubiquitin was purchased from R&D Systems. Luciferase and Goat anti-Luciferase antibody were purchased from Promega.

*Cloning and Vector Construction*

Full-length human pET28a-His<sub>6</sub>-Hsp70<sub>1-641</sub> was a generous gift from J. Gestwicki (UCSF). Expression constructs of His-tagged Ubch5b and Ubiquitin were previously described (Xu et al, 2008a). Human Hsc70<sub>541-646</sub> and Hsc70<sub>541-638</sub> (lid+tail, with and without the C-terminal GPTIEEVD motif respectively) were cloned into the pET151/D-TOPO vector (Invitrogen). The resulting plasmid codes for a His<sub>6</sub> tag and a V5 epitope, followed by a tobacco etch virus (TEV) protease cleavage site, residues GIDPFTEF and the indicated Hsc70 residues. Hsc70<sub>541-646</sub> $\Delta$ <sub>626-638</sub> was constructed by deleting residues 626-638 from the pET151/D-TOPO Hsc70<sub>541-646</sub> template by site-directed mutagenesis. Human Hsc70<sub>395-646</sub> and Hsc70<sub>395-638</sub> (SBD $\beta$ +lid+tail, with and without the C-terminal GPTIEEVD motif respectively) were cloned into the pGSTII2 expression vector (Sheffield et al., 1999); the resulting plasmid, pGSTII2-HsHsc70<sub>395-646</sub>, codes for an N-terminal glutathione-S-transferase tag, tobacco etch virus (TEV) protease cleavage site, residues GAMA, and the indicated Hsc70 residues.

Full-length human CHIP<sub>1-303</sub> was previously described (Xu et al, 2008a). CHIP<sub>21-154</sub> (TPR domain) was PCR-amplified by PCR from the full-length human CHIP construct and cloned into the pHisII2 expression vector (Sheffield et al., 1999); the resulting plasmid codes for a His<sub>6</sub> tag, tobacco etch virus (TEV) protease cleavage site, the residues GAMGS and human CHIP residues 21-154.

All CHIP, Hsc70 and Hsp70 mutants (including short deletions) were made with the QuickChange II Site-Directed Mutagenesis Kit (Agilent). All constructs were verified by sequencing.

### *Protein Expression*

Sequence-verified constructs were transformed into *E. coli* Rosetta2 (DE3) cells (EMD Chemicals) for expression. Expression cultures in Terrific Broth (Research Products International) were grown at 37°C until OD<sub>600</sub> reached 1.0, cooled on ice for 15 minutes, and induced by addition of 250 μM isopropyl β-D-1-thiogalactopyranoside (IPTG). Growth was continued for 20 hours at 18 °C. <sup>15</sup>N-labeled proteins were expressed similarly in vitamin-supplemented buffered media containing 1 g/L <sup>15</sup>N-ammonium chloride (Studier, 2005). Cells expressing full-length His<sub>6</sub>-Hsp70 (residues 1-641) were grown as described above, except that cultures were supplemented with 40 mM glucosamine-HCl (Zachova et al., 2009). Cell pellets were resuspended in 25 mM HEPES (pH 7.0), 50 mM NaCl, 5 mM 2-mercaptoethanol, 1 mg/ml lysozyme (Sigma), 20 μg/ml DNaseI (MP Biomedicals), 100 μg/ml 4-(2-Aminoethyl) benzenesulfonyl fluoride hydrochloride (AEBSF; Gold Biotechnology), with the following exception: the full-length Hsp70 pellet was resuspended with 25 mM HEPES (pH 7.2), 450 mM NaCl, 10 mM MgCl<sub>2</sub>, 1 mM DTT and 10% glycerol. Resuspended cells were flash-frozen in liquid nitrogen and stored at -80 °C.

### *Protein Purification*

Frozen cells suspensions were thawed and lysed overnight with slow rotation at 4 °C. Lysates were clarified by centrifugation at 17,000 *g* for 45 minutes, followed by filtration of lysate supernatants through a .45μM filter (VWR).

His<sub>6</sub>-tagged proteins were purified by Ni<sup>2+</sup>-affinity chromatography using 5mL HisTrap HP columns (GE Healthcare) in 25 mM HEPES (pH 7.6), 50 mM NaCl, eluted in 50-1000 mM imidazole gradients. His<sub>6</sub>-tags of selected proteins were cleaved from proteins by overnight digestion with His<sub>6</sub>-tagged tobacco etch virus (TEV) protease (Kapust and Waugh, 2000) and 5 mM 2-mercaptoethanol and repurified by Ni<sup>2+</sup>-affinity chromatography. Final purification of tagged or untagged proteins was carried out by

size exclusion chromatography on HiLoad 16/60 Superdex 75 or Superdex 200 gel filtration columns (GE Healthcare). Purified proteins were concentrated, frozen drop-wise in liquid nitrogen and stored at -80 °C.

Lysates containing GST-tagged proteins were purified by glutathione affinity chromatography using 5 mL GSTrap HP columns (GE Healthcare). Columns were equilibrated with 25 mM HEPES (pH 7.6), 50 mM NaCl and eluted in 1x PBS (pH 7.5) or 25 mM HEPES (pH 7.6), 10 mM reduced glutathione (Amresco). Peak fractions containing the purified GST-fusion proteins were exchanged into 25 mM HEPES (pH 7.6), 50 mM NaCl and frozen as described above.

Human Uba1 ubiquitin activating enzyme (E1) was purified by activity (Haas et al., 1982; Haas, 2005). Ubiquitin (R&D Systems) was covalently linked to NHS-activated Sepharose HP column (GE Healthcare) following the manufacturer's protocol. The Ub-sepharose column was equilibrated in 25 mM HEPES (pH 7.0), 150 mM NaCl, 0.5 mM DTT. Lysate containing GST~Ube1 fusion protein were loaded onto the Ub-sepharose column in the presence of 2 mM ATP and 10 mM MgCl<sub>2</sub>, washed with 25 mM HEPES (pH 7.0), 150 mM NaCl and eluted in 25 mM HEPES (pH 7.0), 150 mM NaCl and 10 mM DTT. Eluted GST~Uba1, concentrated to 5 μM, was supplemented with glycerol to 10% final concentration, flash frozen and stored at -80 °C.

#### *CHIP/Hsc70-SBD Pull-down Assays*

His-CHIP<sub>1-303</sub> and GST~Hsc70<sub>395-646</sub> constructs, each 40 μM in 50 μl total volume, were incubated on ice for 30 minutes. Following the incubation period His-Mag Sepharose Ni beads (GE Healthcare) were added. The supernatant was removed and beads were washed four times with 400 μl 50 mM HEPES, pH 7.0, 50 mM NaCl. Aliquots of CHIP, GST~Hsc70, final wash supernatant and elution fractions were separated by SDS-PAGE with detection by Coomassie staining.

#### *NMR Spectroscopy*

NMR spectra were collected at 25°C on Bruker Avance spectrometers at 600 MHz or 850 MHz. Bruker 600 MHz and 850 MHz spectrometers were equipped with a room temperature probes. Prior to titration, both <sup>15</sup>N-labeled proteins and natural

abundance (unlabeled) proteins were dialyzed against the same batch of buffer. Final samples contained 20 mM HEPES (pH 7.0) and 20 mM NaCl and 10% D<sub>2</sub>O. Concentrations of <sup>15</sup>N-labeled proteins are listed in the Supplemental Figure legends. Two dimensional <sup>1</sup>H/<sup>15</sup>N-HSQC spectra were acquired using a spin-state selective gradient-enhanced HSQC pulse sequence (Schleucher et al., 1994). All datasets were processed using in-house scripts for NMRPipe (Delaglio et al., 1995) and analyzed with Sparky.

### *Hsp70-Chaperoned Luciferase Ubiquitination Assays*

Firefly luciferase was incubated at 25°C for 10 minutes and heat-denatured at 45°C for 10 minutes in the presence of 5 μM Hsp70, 5 μM Hsp40 and 5 μM Bag2<sub>107-189</sub> (Bag2 BNB domain (Xu et al., 2008b)). Simultaneously, an E2~Ub conjugate charging reaction was incubated at 37°C for 20 minutes. Heat denatured luciferase was cooled to 4°C and pooled with pre-charged E1/E2~Ub reactions and CHIP in luciferase ubiquitination reactions consisting of 2 μM luciferase, 2.5 μM Hsp70, 2.5 μM Hsp40, 2.5 μM Bag2<sub>107-189</sub>, 1 μM CHIP, 0.5 μM E1, 40 μM UbcH5b, 200 μM Ub, 20 mM ATP, 40 mM MgCl<sub>2</sub> and 0.5 mM DTT in a buffer containing 20 mM HEPES (pH 7.0) and 50 mM NaCl. All reactions were quenched at specified time points by addition of 2x SDS sample buffer with 20 mM DTT, and analyzed by SDS PAGE and Western Blotting with near-infrared detection using Goat anti-luciferase (Promega) primary and Donkey anti-Goat IRDye680-labeled secondary (LI-COR) antibody.

### *Generation of Docking Models for Hsc70-Lid/TPR Complexes*

Models of Hsc70-lid in complex with TPR domains of CHIP, Hop and SGTA were generated with Rosetta Dock. Initial poses for the docking calculations were prepared by aligning human Hop TPR1 (PDB code 1ELW; Scheufler et al., 2000), a human homology model of yeast Hop TPR2B (PDB code 3UPV; Schmid et al., 2012) and human SGTA TPR1-3 (PDB code 2VYI; Dutta and Tan, 2008). The homology model for human Hop TPR2B was generated using I-TASSER (Roy et al., 2010) and had a C-score of 1.29. To allow fuller exploration of local energy minima, no docking constraints were used. Docking simulations utilized the Rosetta Dock v3.4 high-resolution local

docking refinement mode (Chaudhury et al., 2011) and produced a family of 1500 decoys for each complex. Docking runs were considered to have converged if a docking funnel was achieved and the number of near-native decoys among the five lowest energy decoys ( $N_5$ ) is greater than or equal to three ( $N_5 \geq 3$ , Chaudhury et al., 2011). A group of the five lowest energy decoys for each run with all atom rmsd ( $AA_{\text{rmsd}}$ ) to the lowest energy decoy of  $< 1 \text{ \AA}$  were considered to be high quality,  $1 \text{ \AA} < AA_{\text{rmsd}} < 2 \text{ \AA}$  were considered medium quality and  $2 \text{ \AA} < AA_{\text{rmsd}} < 4 \text{ \AA}$  were judged to be acceptable quality (Chaudhury et al., 2011).

**Supplemental References**

- Delaglio, F., Grzesiek, S., Vuister, G.W., Zhu, G., Pfeifer, J., and Bax, A. (1995). NMRPipe: a multidimensional spectral processing system based on UNIX pipes. *J. Biomol. NMR* *6*, 277–293.
- Haas, A.L., Warms, J.V., Hershko, A., and Rose, I.A. (1982). Ubiquitin-activating enzyme. Mechanism and role in protein-ubiquitin conjugation. *J. Biol. Chem.* *257*, 2543–2548.
- Haas, A.L. (2005). Purification of E1 and E1-like enzymes. *Methods Mol. Biol.* *301*, 23–35.
- Kapust, R.B., and Waugh, D.S. (2000). Controlled intracellular processing of fusion proteins by TEV protease. *Protein Expres. Purif.* *19*, 312–318.
- Krissinel, E., and Henrick, K. (2007). Inference of macromolecular assemblies from crystalline state. *J. Mol. Biol.* *372*, 774–797.
- Roy, A., Kucukural, A., and Zhang, Y. (2010). I-TASSER: a unified platform for automated protein structure and function prediction. *Nat. Protoc.* *5*, 725–738.
- Schleucher, J., Schwendinger, M., Sattler, M., Schmidt, P., Schedletzky, O., Glaser, S.J., Sørensen, O.W., and Griesinger, C. (1994). A general enhancement scheme in heteronuclear multidimensional NMR employing pulsed field gradients. *J. Biomol. NMR* *4*, 301–306.
- Schrödinger LLC. PyMOL Molecular Graphics System, Version 1.6.0.0. Pymol.Sourceforge.Net.
- Sheffield, P., Garrard, S., and Derewenda, Z. (1999). Overcoming expression and purification problems of RhoGDI using a family of “parallel” expression vectors. *Protein Expres. Purif.* *15*, 34–39.
- Studier, F.W. (2005). Protein production by auto-induction in high density shaking cultures. *Protein Expres. Purif.* *41*, 207–234.
- Zachova, K., Krupka, M., Chamrad, I., Belakova, J., Horynova, M., Weigl, E., Sebela, M., and Raska, M. (2009). Novel modification of growth medium enables efficient *E. coli* expression and simple purification of an endotoxin-free recombinant murine hsp70 protein. *J. Microbiol. Biotechnol.* *19*, 727–733.